

Tuning a magnetic energy scale with pressure in UTe_2

Hyunsoo Kim,^{1,*} I-Lin Liu,¹ Wen-Chen Lin,¹ Yun Suk Eo,¹
Sheng Ran,¹ Nicholas P. Butch,^{1,2} and Johnpierre Paglione^{1,3}

¹*Maryland Quantum Materials Center and Department of Physics,
University of Maryland, College Park, Maryland, USA*

²*NIST Center for Neutron Research, National Institute of Standards and Technology, Gaithersburg, MD 20899, USA*

³*Canadian Institute for Advanced Research, Toronto, Ontario M5G 1Z8, Canada[†]*

(Dated: July 4, 2023)

A fragile ordered state can be easily tuned by various external parameters. When the ordered state is suppressed to zero temperature, a quantum phase transition occurs, which is often marked by the appearance of unconventional superconductivity. While the quantum critical point can be hidden, the influence of the quantum criticality extends to fairly high temperatures, manifesting the non-Fermi liquid behavior in the wide range of the p - H - T phase spaces. Here, we report the tuning of a magnetic energy scale in the heavy-fermion superconductor UTe_2 , previously identified as a peak in the c -axis electrical transport, with applied pressure and magnetic field as complementary tuning parameters. Upon increasing pressure, the characteristic c -axis peak moves to a lower temperature before vanishing near the critical pressure of about 15 kbar. The application of a magnetic field broadens the peak under all studied pressure values. The observed Fermi-liquid behavior at ambient pressure is violated near the critical pressure, exhibiting nearly linear resistivity in temperature and an enhanced pre-factor. Our results provide a clear picture of energy scale evolution relevant to magnetic quantum criticality in UTe_2 .

Unconventional superconductivity is often found in the vicinity of a fragile long-range magnetic order (LRMO) [1]. When LRMO is suppressed by either chemical substitutions, magnetic field or physical pressure, the system undergoes a quantum phase transition at a critical value of the tuning parameter [2, 3]. However, the quantum critical point (QCP) is often hidden inside a dome of the superconducting instability around QCP. The pairing glue responsible for this superconductivity is associated with LRMO, giving rise to the magnetically mediated superconducting state. While the majority of magnetic unconventional superconductors are found near the antiferromagnetic instability, several uranium-based superconductors including URhGe and UCoGe coexist with ferromagnetism [4], making them promising candidates for a topological spin-triplet superconductor. Recently, UTe_2 joined as a new U-based superconductor [5], and its T_c is as high as 2 K [6]. The normal state of UTe_2 can be best described by the Kondo lattice where the localized magnetic moment of uranium is hybridized with the conduction electrons at low temperatures. UTe_2 does not magnetically order, but the superconductivity in this paramagnetic heavy fermion is believed to be in the vicinity of the magnetic instability [5]. The application of moderate pressure induces a long-range magnetic order [7]. Because of the relatively small energy scales of the superconductivity and LRMO in UTe_2 , it displays a rich phase diagram when the system is subjected to external parameters. However, the understanding of competition and interplay between magnetism and superconductivity in UTe_2 remains elusive. Furthermore, the nature of QCP is not transparent.

In this work, we investigate electrical transport prop-

erties in UTe_2 to elucidate its quantum criticality and relevant energy scales by tuning a magnetic field and pressure. We measured the electrical resistance R with the current along the crystallographic c -axis [8] under pressure up to 17.4 kbar and in magnetic fields up to 18 T. We determined the pressure and field evolution of the characteristic c -axis peak, $H_{c2(T)}$, and the power-law behavior of the c -axis electrical resistance. Our results clearly show energy scale evolution relevant to magnetic quantum criticality in UTe_2 .

Figure 1 shows the electrical resistance $R(T)$ in UTe_2 with the current along the crystallographic c -axis at various applied pressures up to $p = 17.4$ kbar. The ambient pressure (0 kbar) $R(T)$ curve, possibly affected by the residual strain in the pressure cell, exhibits the characteristic c -axis peak around 13 K [11]. Panel (a) shows that the peak monotonically moves towards the lower temperature with increasing pressure. Inset in panel (a) shows the pressure evolution of the resistive superconducting transition. The application of small pressure of 0.5 kbar slightly lowers T_c , but subsequent higher pressures enhance T_c . The maximum T_c was observed at $p = 9.7$ kbar above which T_c rapidly decreases. Superconductivity was observed up to 14.2 kbar. The resistive superconducting transition in $R(T)$ exhibits distinct features under different pressures. The $R(T)$ with 0 and 0.5 kbar exhibits a shoulder-like feature in the transition (black and red curves), which may be associated with the double transitions observed in heat capacity measurements [12–14]. The $R(T)$ curves with $p = 0.5, 5.3, 7.5$, and 9.7 kbar exhibit an upturn before the superconducting transition upon cooling. At $p = 9.7$ kbar, the resistive superconducting transition is the sharpest. At

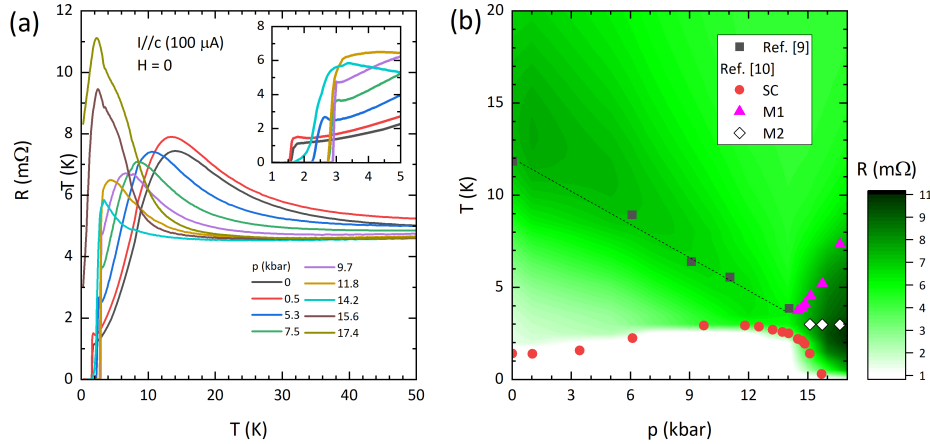


FIG. 1. **Pressure evolution of low-temperature $R(T)$ in UTe_2 with $I \parallel c$ -axis in the absence of a magnetic field.** Panel (a) shows $R(T)$ in UTe_2 with the electrical current along the crystallographic c -axis at various applied pressures up to $p = 17.4$ kbar. The c -axis peak monotonically moves towards the lower temperature with increasing pressure. Inset: pressure evolution of the resistive superconducting transition. Panel (b) shows $R(T, p)$ which displays the pressure evolution of the c -axis peak spectacularly. The characteristic temperatures are overlaid on the plot. The red and black symbols represent the superconducting transition [9] and a shoulder-like feature in χ_a [10], respectively. The triangle and diamond symbols observed above 14.5 kbar are associated with a long-range magnetic ordering [9]. We found that the pressure evolution of the c -axis peak coincides with the pressure evolution of χ_a , which suggests its magnetic origin in nature.

$p = 14.2$ kbar, the transition becomes very broad with a long tail, and $R(T)$ gradually becomes zero well below the onset of the superconducting transition. Above $p \approx 15.6$ kbar, low-temperature $R(T)$ curves exhibit a substantial increase with the shoulder-and peak-like features below which $R(T)$ decreases rapidly. Superconductivity was not observed down to $T \approx 0.3$ K for both 15.6 and 17.4 kbar.

Figure 1(b) shows $R(T, p)$, which displays the pressure evolution of the c -axis peak spectacularly. The darker green indicates the larger electrical resistance. The relatively wide c -axis peak around 13 K at 0 kbar moves to lower temperatures, and the feature becomes narrower. The characteristic temperatures are overlaid on the plot with symbols. The red and black symbols represent the superconducting transition [9] and a shoulder-like feature in χ_a [10], respectively. The triangle and diamond symbols observed above 14.5 kbar are associated with a long-range magnetic ordering [9]. We found that the pressure evolution of the c -axis peak coincides with the pressure evolution of χ_a , which suggests its magnetic origin in nature. We note that the $R(T)$ data shown in Fig. 1 were taken with a fixed current $I = 0.1$ mA.

Figure 2(a-e) shows the field-evolution of $R(T)$ with applied pressure from 5.3 kbar to 14.2 kbar where $R(T)$ curves exhibit a local maximum. We define T^* and R^* which respectively correspond to the temperature and resistance at the c -axis peak, and they represent the field-evolution of the low-temperature scattering rate at each pressure. The field-dependent T^* and R^* show common features at all pressures. First, R^* decreases with the field, and the peak evolves to a broad feature at high magnetic fields. Second, T^* increases as the field in-

creases. The field-dependence of T^* and R^* at various pressures is summarized in panels (f) and (g), respectively. T^* monotonically increases with the field, and the field-dependence becomes virtually linear above 6 T. The increasing rate $dT^*/d(\mu_0 H)$ determined with a field range between 6 T and 18 T is shown in panel (h) as a function of the applied pressure. The pressure evolution of $dT^*/d(\mu_0 H)$ is nearly linear. On the other hand, R^* generally decreases with the field in all applied pressure. At low fields, it is weakly field-dependent. In $p = 14.2$ kbar, it is nearly field-independent up to 4 T. Above 6 T, R^* varies as $a^*(H + H_0)^{-1}$ where a^* and H_0 depend on the pressure. a^* corresponds to the field-suppression rate of R^* , and its pressure variation is shown in panel (h).

Figure 3(a) shows the temperature-dependent upper critical field $H_{c2}(T)$ at various pressures. The $H_{c2}(T)$ curves were determined from $R(T)$ measurements with the electrical current along the c -axis and the magnetic field applied parallel to the a -axis at the applied pressures up to $p = 14.2$ kbar. We used the zero resistance criteria for the superconducting transition temperature T_{sc} . While the $H_{c2}(T)$ curve without the applied pressure exhibits a smooth variation, the application of pressure drastically changes the shape of the superconducting H - T phase lines. Near T_c , the slope of $H_{c2}(T)$ increases by almost five-fold with pressure at $p = 9.7$ kbar, and it slightly decreases at 11.8 kbar. Surprisingly, the application of 14.2 kbar induces reentrant behavior of superconductivity. The large slope change of $H_{c2}(T)$ at T_c with pressure indicate the significant variation in the orbital limiting $H_{c2}(0)$ [15]. However, the overall observed

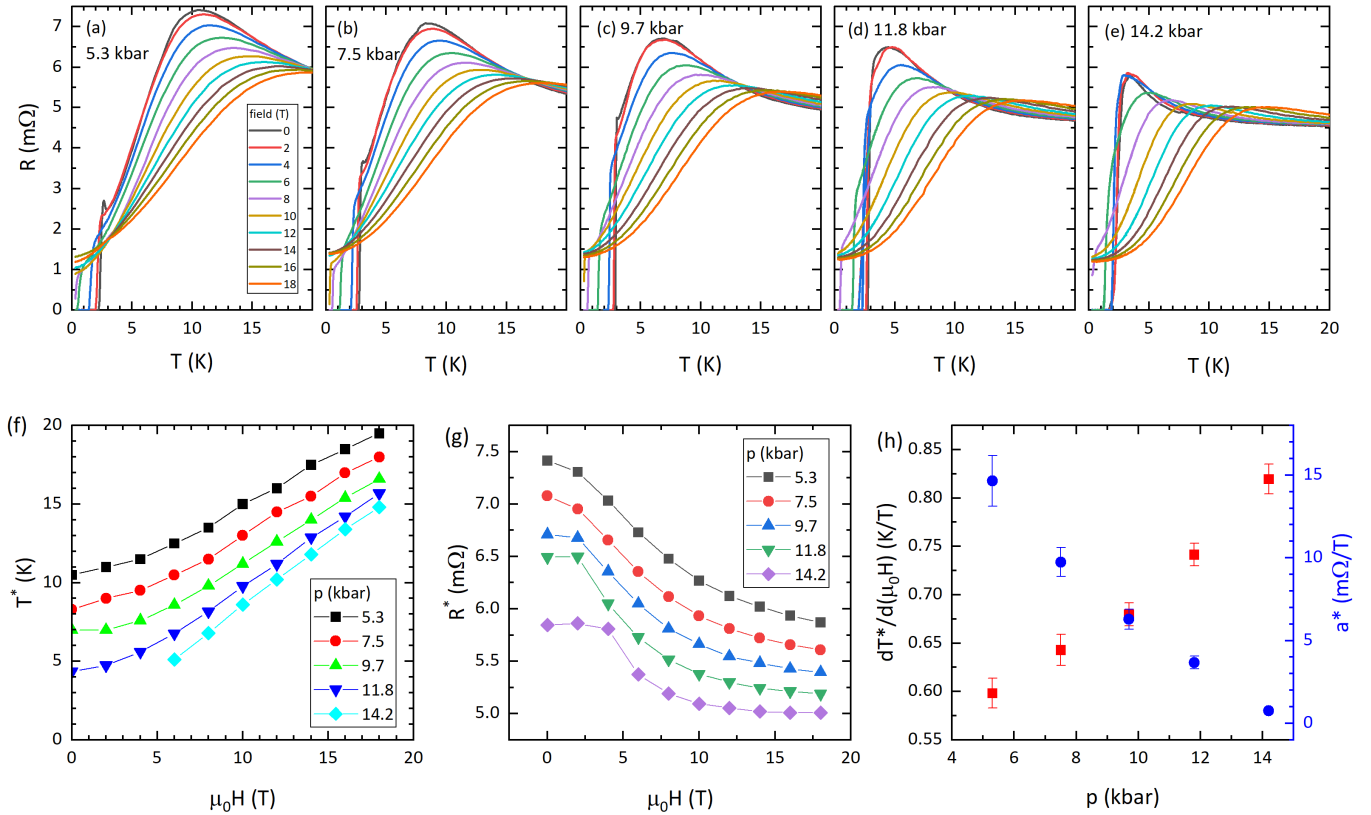


FIG. 2. **Magnetic field evolution of low-temperature $R(T)$ in UT_2 at various pressures.** Panels (a-e) show the field-evolution of $R(T)$ with applied pressure from 5.3 kbar to 14.2 kbar where $R(T)$ curves exhibit a local maximum. We define T^* and R^* which respectively correspond to the temperature and resistance at the c -axis peak. The field-dependent T^* and R^* show common features at all pressures, which are summarized in panels (f) and (g). Above 6 T, R^* varies as $a^*(H + H_0)^{-1}$ where a^* and H_0 depend on the pressure. a^* corresponds to the field-suppression rate of R^* , and its pressure variation is shown in panel (h).

$\mu_0 H_{c2}(T)$ at the lowest temperature remains around 8 ± 2 T as shown in panel (a). When the field-driven superconducting to normal state transition occurs due to the orbital limiting effect, $H_{c2}(0)$ can be estimated from $|dH_{c2}/dT|_{T_c}$ with a relation, $H_{c2}(0) = -\lambda T_c dH_{c2}/dT$ at T_c [15]. Here $\lambda \approx 0.73$ and 0.69, which correspond to the clean and dirty limits, respectively [15, 16]. Alternatively, the spin-singlet superconductivity can be suppressed due to Pauli paramagnetism, and the limiting value H_P can be estimated by the relation, $H_P = \Delta_0/\sqrt{2}\mu_B$. Here Δ_0 and μ_B are the magnitudes of the superconducting energy gap at zero temperature and the Bohr magneton, respectively. For the weak-coupling BCS superconductor, $\mu_0 H_P = \alpha T_c$ where $\alpha \approx 1.87$ T/K.

Figure 3(b) compares the experimental $H_{c2}(0)$ to both limiting fields, H_{HW} and H_P . Figure 3(c) shows the pressure evolution of $H_{HW}/H_{c2}(0)$ and $H_P/H_{c2}(0)$. While H_P remains less than $H_{c2}(0)$, indicating non-singlet pairing, H_{HW} exhibits a substantial variation. The large H_{HW} prediction is generally evidence for the heavy-fermion normal state. The pressure-evolution of H_{HW} , which exhibits a significant enhancement around 10 kbar,

indicates increasing effective mass with pressure. However, the orbital limiting effective is interrupted, and the largest discrepancy between $H_{c2}(0)$ and H_{HW} is observed at 9.7 kbar where the highest T_c is observed. A similar effect was observed in other heavy fermion superconductors near the quantum critical point, suggesting the existence of QCP near 10 kbar. At low temperatures, a drastic slope change appears at low temperatures for the pressure between 5.3 and 11.8 kbar. The slope change in UTe_2 was previously reported by Aoki et al., which was attributed to the existence of other superconducting phases [13]. A similar $H_{c2}(T)$ behavior was reported by Kasahara et al. in FeSe [17], which was attributed to the Fulde–Ferrell–Larkin–Ovchinnikov (FFLO) state [18–20].

We found the width of the superconducting phase transition in resistivity is closely related to this anomalous behavior in $H_{c2}(T)$. To shed light on the origin of this feature, we determined the field-dependent transition width compared to the T_{sc} that is determined at the zero resistivity, $\Delta T_c/T_{sc}$. In all studied pressure, $\Delta T_c/T_{sc}$ exhibits strong enhancement where the sudden slope change oc-

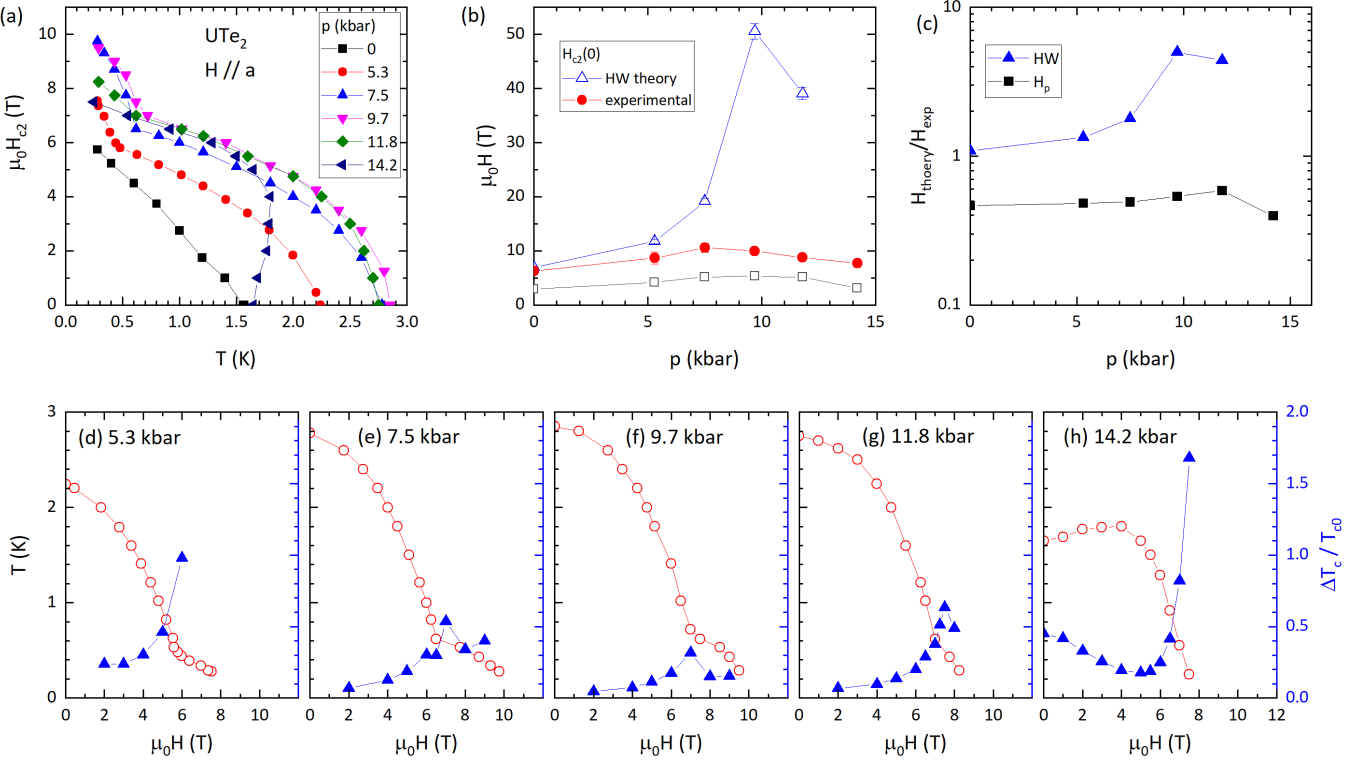


FIG. 3. **Superconducting H - T phase diagram in UTe_2 with H along the a -axis at various pressures.** Panel (a) shows the temperature-dependent upper critical field $H_{c2}(T)$ at various pressures, using the zero resistance criteria for the superconducting transition temperature T_{sc} . Panel (b) compares the experimental $H_{c2}(0)$ to the orbital limiting field, HH_W , and the paramagnetic limiting field, H_P . Panel (c) shows the pressure evolution of $H_{HW}/H_{c2}(0)$ and $H_P/H_{c2}(0)$. We found the width of the superconducting phase transition in resistivity is closely related to this anomalous behavior in $H_{c2}(T)$. Under all studied pressure, $\Delta T_c/T_{sc}$ exhibits strong enhancement where the sudden slope change occurs as shown in panels (d-h). It is notable that $\Delta T_c/T_{sc}$ decreases above H^* in $p = 7.5, 9.7, 11.8$ kbar where the low-temperature data above H^* are available.

curs as shown in panels (d-h). We define H^* where the slope of $H_{c2}(T)$ changes. It is notable that $\Delta T_c/T_{sc}$ decreases above H^* in $p = 7.5, 9.7, 11.8$ kbar where the low-temperature data above H^* are available. The broad superconducting transition is usually associated with inhomogeneity [9, 21, 22] or a filamentary superconducting state. However, the systematic field dependence rules out these simple scenarios.

Figure 4(a-e) shows the field-dependent exponent n^* of the low-temperature $R(T)$ determined under various pressures by a relation, $n^* = d[\log(\rho(T) - \rho_0)]/d[\log T]$. $R(0)$ is estimated by extrapolating the $R(T)$ tail by assuming a power-law of low-temperature $R(T)$. Provided $R(0)$ is accurate, n^* is equivalent with the exponent from the power-law, $R(T) = R(0) + AT^n$. In the study by Eo et al., the Fermi liquid (FL) behavior, i.e., $n = 2$, in the c -axis transport was reported in the absence of both field and applied pressure [11]. Here we focus on the pressures between 5.3 kbar and 14.2 kbar. At 5.3 kbar, it exhibits the FL behavior (yellow) just above T_c in $H = 0$, but the low temperature n^* decreases down to $n^* \approx 1.5$ (light green) with increasing field near $H_{c2}(0)$. At 7.5 kbar and 9.7 kbar, while the c -axis transport exhibits the non-FL

behavior near $H_{c2}(0)$, the FL behavior (yellow) is recovered at high fields between 15 T and 18 T. At 11.8 kbar and 14.2 kbar, the exponent reached $n = 2.5$ (red) at high fields.

We performed least-square fitting on selected $R(T)$ curves by fitting a relation $R(T) = R(0) + AT^n$ to the experimental data with $T \leq T^*/2$. The fitting results for n and A are summarized as a function of the field in panels (f,g) and pressure in panels (h,i). For $p = 5.3$ kbar, $n = 2$ in the absence of the field. However, it shows a smooth variation with the field, showing a minimum value of $n = 1.5$ near 10 T. It weakly increases at high fields. while it remains sub-quadratic at 11 T. For the higher pressures between 7.5 and 11.8 kbar, a more drastic decrease in n with a minimum near 6-8 T where the $H_{c2}(T)$ changes the slope. The lowest exponent $n \approx 1$ is observed near x T at 9.7 kbar. At higher fields, n increases substantially to about 2.5 for 11 kbar and 14.2 kbar. The A -the coefficient is correlated with n showing significant enhancement around 6-10 T. Panels (h, i) show the pressure variation of n and A as a function of pressure at each fixed field. The appearance of a dip in n and a peak in A at a field near the suppression of

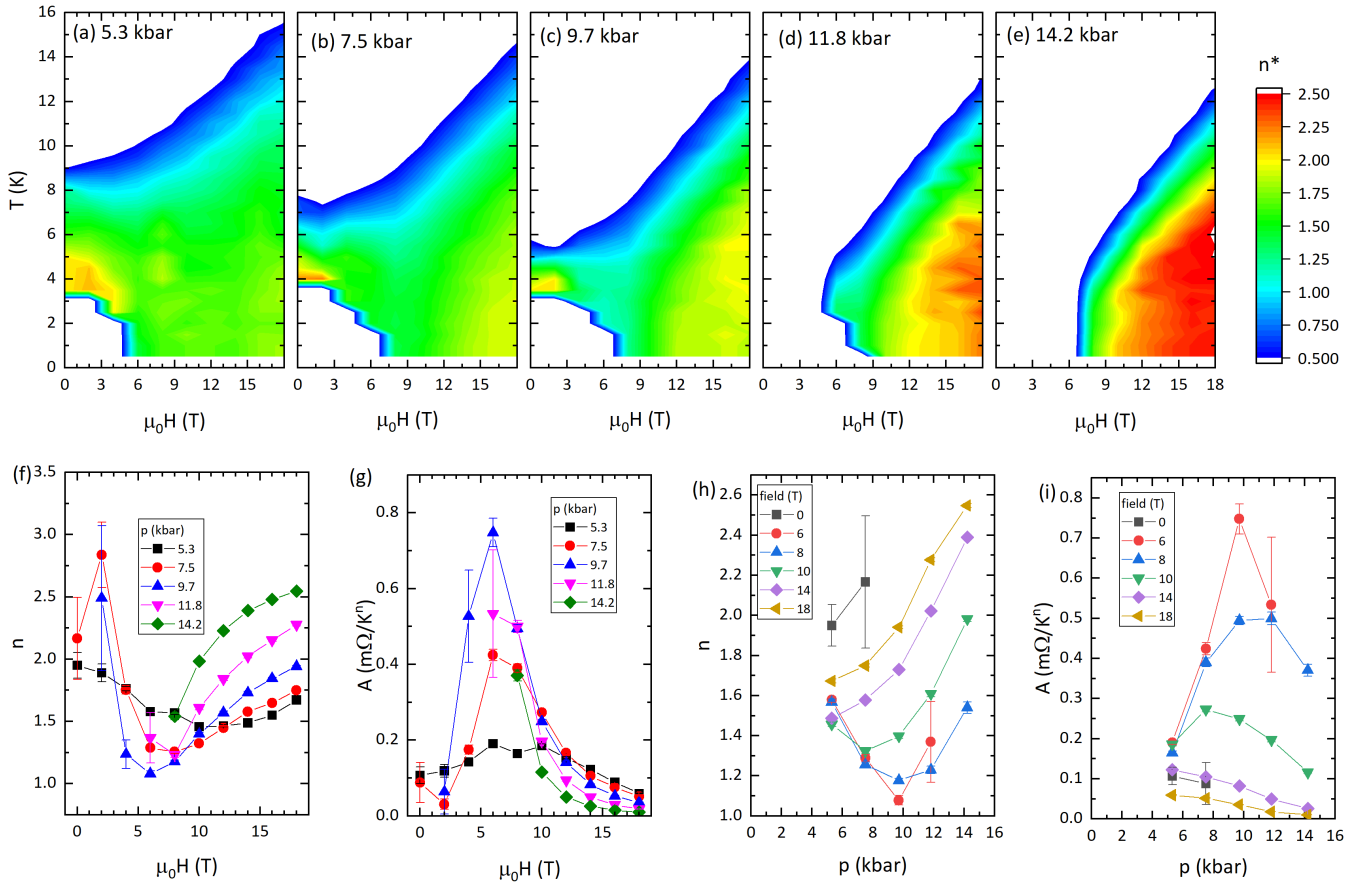


FIG. 4. **Field-and pressure-evolution of the power-law behavior of low-temperature $R(T)$ in UTe_2 .** Panels (a-e) show the field-dependent exponent n^* of the low-temperature $R(T)$ determined under various pressures by a relation, $n^* = d[\log(\rho(T) - \rho_0)]/d[\log T]$. Here we focus on the pressures between 5.3 kbar and 14.2 kbar. At 5.3 kbar, it exhibits the FL behavior (yellow) just above T_c in $H = 0$, but the low temperature n^* decreases down to $n^* \approx 1.5$ (light green) with increasing field near $H_{c2}(0)$. We performed least-square fitting on selected $R(T)$ curves by fitting a relation $R(T) = R(0) + AT^n$ to the experimental data with $T \leq T^*/2$. The fitting results for n and A are summarized as a function of the field in panels (f,g) and pressure in panels (h,i). Panels (h, i) show pressure variation of n and A as a function of pressure at each fixed field. The appearance of a dip in n and a peak in A at a field near the suppression of the superconducting state is a typical manifestation of a quantum critical point in the electrical transport property.

the superconducting state is a typical manifestation of a quantum critical point in the electrical transport property. In a typical metal, Fermi liquid behavior or T^2 at low temperatures. The exponent less than 2 or non-Fermi liquid behavior signals unconventional scattering due to enhanced spin fluctuations often near a magnetic quantum critical point. Recently, $n = 1$ was reported by Thomas et al. in Ref. [14].

In summary, we investigate electrical transport properties in UTe_2 to elucidate its quantum criticality and relevant energy scales by tuning a magnetic field and pressure. We measured the electrical resistance R with the current along the crystallographic c -axis under pressure up to 17.4 kbar and magnetic fields up to 18 T. We found the temperature of the characteristic c -axis peak decreases with increasing pressure accompanied by decreasing R value at the peak. It is no longer discernible

above 14.2 kbar where the resistance values are substantially increased due to the appearance of an apparent long-range magnetic ordering. The peak rapidly broadens with the increasing field, and the peak R -value decreases while moving to a higher temperature. The superconducting H - T phase diagrams are constructed at each pressure, and the estimated $H_{c2}(0)$ values are compared to the orbital and Pauli limiting fields. Overall, $H_{c2}(T)$ exhibits anomalous behavior by changing its slope, including reentrance of superconductivity at 14.2 kbar. We observed that the superconducting transition becomes very broad where the slope changes at all measured pressure values. We examined the power-law behavior in the H - p phase space and found the signatures of typical behavior from the magnetic quantum critical point where the A -coefficient and the exponent n exhibit the maximum and minimum, respectively.

The authors are grateful for the useful discussions with Andriy Nevidomskyy. Research at the University of Maryland was supported by the Department of Energy Award No. DE-SC-0019154 (transport experiments), the Gordon and Betty Moore Foundation's EPiQS Initiative through Grant No. GBMF9071 (materials synthesis), NIST, and the Maryland Quantum Materials Center.

* Present affiliation: Department of Physics, Missouri University of Science and Technology, Rolla, MO 65409, USA

† paglione@umd.edu

- [1] N. D. Mathur, F. M. Grosche, S. R. Julian, I. R. Walker, D. M. Freye, R. K. W. Haselwimmer, and G. G. Lonzarich, *Nature* **394**, 39 (1998).
- [2] O. Stockert and F. Steglich, *Annual Review of Condensed Matter Physics* **2**, 79 (2011), <https://doi.org/10.1146/annurev-conmatphys-062910-140546>.
- [3] T. Shibauchi, A. Carrington, and Y. Matsuda, *Annual Review of Condensed Matter Physics* **5**, 113 (2014), <https://doi.org/10.1146/annurev-conmatphys-031113-133921>.
- [4] D. Aoki, K. Ishida, and J. Flouquet, *Journal of the Physical Society of Japan* **88**, 022001 (2019), <https://doi.org/10.7566/JPSJ.88.022001>.
- [5] S. Ran, C. Eckberg, Q.-P. Ding, Y. Furukawa, T. Metz, S. R. Saha, I.-L. Liu, M. Zic, H. Kim, J. Paglione, and N. P. Butch, *Science* **365**, 684 (2019).
- [6] P. F. S. Rosa, A. Weiland, S. S. Fender, B. L. Scott, F. Ronning, J. D. Thompson, E. D. Bauer, and S. M. Thomas, [arXiv:2110.06200](https://arxiv.org/abs/2110.06200) (2021).
- [7] S. Ran, H. Kim, I.-L. Liu, S. R. Saha, I. Hayes, T. Metz, Y. S. Eo, J. Paglione, and N. P. Butch, *Phys. Rev. B* **101**, 140503 (2020).
- [8] Y. S. Eo, S. Liu, S. R. Saha, H. Kim, S. Ran, J. A. Horn, H. Hodovanets, J. Collini, T. Metz, W. T. Fuhrman, A. H. Nevidomskyy, J. D. Denlinger, N. P. Butch, M. S. Fuhrer, L. A. Wray, and J. Paglione, *Phys. Rev. B* **106**, L060505 (2022).
- [9] S. M. Thomas, C. Stevens, F. B. Santos, S. S. Fender, E. D. Bauer, F. Ronning, J. D. Thompson, A. Huxley, and P. F. S. Rosa, *Phys. Rev. B* **104**, 224501 (2021).
- [10] D. Li, A. Nakamura, F. Honda, Y. J. Sato, Y. Homma, Y. Shimizu, J. Ishizuka, Y. Yanase, G. Knebel, J. Flouquet, and D. Aoki, *Journal of the Physical Society of Japan* **90**, 073703 (2021), <https://doi.org/10.7566/JPSJ.90.073703>.
- [11] Y. S. Eo, S. R. Saha, H. Kim, S. Ran, J. A. Horn, H. Hodovanets, J. Collini, W. T. Fuhrman, A. H. Nevidomskyy, N. P. Butch, M. S. Fuhrer, and J. Paglione, [arXiv:2101.03102](https://arxiv.org/abs/2101.03102) (2021).
- [12] D. Braithwaite, M. Vališka, G. Knebel, G. Lapertot, J. P. Brison, A. Pourret, M. E. Zhitomirsky, J. Flouquet, F. Honda, and D. Aoki, *Communications Physics* **2**, 147 (2019).
- [13] D. Aoki, F. Honda, G. Knebel, D. Braithwaite, A. Nakamura, D. Li, Y. Homma, Y. Shimizu, Y. J. Sato, J.-P. Brison, and J. Flouquet, *Journal of the Physical Society of Japan* **89**, 053705 (2020), <https://doi.org/10.7566/JPSJ.89.053705>.
- [14] S. M. Thomas, F. B. Santos, M. H. Christensen, T. Asaba, F. Ronning, J. D. Thompson, E. D. Bauer, R. M. Fernandes, G. Fabbris, and P. F. S. Rosa, *Science Advances* **6**, 10.1126/sciadv.abc8709 (2020).
- [15] E. Helfand and N. R. Werthamer, *Phys. Rev.* **147**, 288 (1966).
- [16] V. G. Kogan and R. Prozorov, *Reports on Progress in Physics* **75**, 114502 (2012).
- [17] S. Kasahara, Y. Sato, S. Licciardello, M. Čulo, S. Arsenijević, T. Ottenbros, T. Tominaga, J. Böker, I. Eremin, T. Shibauchi, J. Wosnitza, N. E. Hussey, and Y. Matsuda, *Phys. Rev. Lett.* **124**, 107001 (2020).
- [18] P. Fulde and R. A. Ferrell, *Phys. Rev.* **135**, A550 (1964).
- [19] A. I. Larkin and Y. N. Ovchinnikov, *Zh. Eksperim. i Teor. Fiz.* **47**, 1136 (1964).
- [20] Y. Matsuda and H. Shimahara, *Journal of the Physical Society of Japan* **76**, 051005 (2007), <https://doi.org/10.1143/JPSJ.76.051005>.
- [21] R. Casalbuoni and G. Nardulli, *Rev. Mod. Phys.* **76**, 263 (2004).
- [22] T. Park, H. Lee, I. Martin, X. Lu, V. A. Sidorov, K. Gofryk, F. Ronning, E. D. Bauer, and J. D. Thompson, *Phys. Rev. Lett.* **108**, 077003 (2012).